Reduced Order Model for Nonlinear Multi-Field-Coupled Spinning Shaft During Transient Operation Based on Coupled Modes Extracted by POD

Mohammad A. Bani-Khaled (banikhaled@gmail.com)
Applied Science Private University https://orcid.org/0000-0002-5033-3140
Ioannis Georgiou
National Technical University of Athens: Ethniko Metsobio Polytechneio

Research Article

Keywords: Proper orthogonal Decomposition (POD), Model Reduction, Spinning Shaft, Coupled Dynamics

Posted Date: March 13th, 2021

DOI: https://doi.org/10.21203/rs.3.rs-304323/v1

Reduced Order Model for Nonlinear Multi-Field-Coupled Spinning Shaft During Transient Operation Based on Coupled Modes Extracted by POD

Reduced Order Model for Nonlinear multi-field-coupled Spinning shaft during transient operation based on coupled modes extracted by POD

Mohammad A. Bani-Khaled[1] , I.T Georgiou[2]

Keywords: Proper orthogonal Decomposition (POD), Model Reduction, Spinning Shaft, Coupled Dynamics

Abstract. Processing the numerical solution for the nonlinear spinning shaft using the Time-(Proper Orthogonal Decomposition) transform identifies the coupling between the rigid body motion and deformation as well as the coupling between the deformation modes. Laying on the fact that the POD characterizes the motion into set of optimum coupled modes, it is convenient to relay on them to derive nonlinear reduced order models. In this work, the discrete dynamics of nonlinear spinning shaft are processed using the POD method to produce optimum modes that are used to furnish bases to derive nonlinear coupled reduced model. The derived reduced model is tested at several operational conditions and compared to the full model characteristics. The reduced model produces back the dynamics; captures the natural frequencies and whirling.

INTRODUCTION

A considerable amount of coupling between the rigid body motion and deformation (straining) may occur in flexible spinning shafts. For linear systems, the motion can be characterized using the normal modes of vibration, while onlinear systems, it is difficult to compute the nonlinear-normal modes of vibrations since the motion is composed of strongly coupled multi-fields. Reduced models in most studies uses the modes of the linearized system as bases for projection. Such approach works for near-linear problems. For nonlinear problems, to derive optimal models, it is necessary to identify the coupled normal modes of vibration. The nonlinear finite element analysis can solve and simulate accurately the nonlinear dynamics of spinning shafts producing numerical databases that contains all necessary data about the motion. If the POD used to process the FEA numerical solution obtained from the nonlinear analysis, then it is possible to extract optimal modes that can be used as base to derive optimal reduced order model.

This paper will use the POD for multi-field coupled dynamics developed by Georgiou [1,2] to study the coupled vibrations of a nonlinear spinning shaft. It is expected that POD will decompose optimally the total overall motion into Proper Orthonormal Modes and provide a mean to quantify the level of

[1] Assistant Professor, Applied Sciences Private University, Jordan, banikhaled@gmail.com. Corresponding author

[2] Professor, National Technical University of Athens, Greece, georgiou@central.ntua.gr

coupling between rigid body motion and straining motions. Also, it will characterize the interaction between axial, bending and torsional vibrations during whirling of shaft. Then the optimal POD mode shapes are used to derive reduced models for whirling motion.

In literature, the study of the dynamics of the rotating shaft is based on the theories of lateral vibration of beams. Bernoulli-Euler model is used for slender shaft with basic assumption that the shaft-cross section remains flat plane and perpendicular to the centerline during the deformation of the shaft. Timoshenko model takes into consideration the rotary inertia of the section plane and shear deformation which have significant effect for thick beams [3-5]. El-Absy , Shabana and Yoo [6,7] studied the coupling between the rigid body and deformation modes in rotating structures that undergoes overall motions.

The occurrence of nonlinear resonances and the effect of bearing directed the researchers to study the nonlinear dynamics of spinning shaft. Yamamoto [8] studied the nonlinear resonances and reported subharmonic resonances due to the ball bearing. Tondl [9] studied the nonlinear resonances due to oil films in the journal bearings. Ehrich [10] reported the occurrence of various types of subharmonic harmonics up to very high order and chaotic vibrations in some aircraft gas turbines.

The presence of cracks in rotating shafts produce complicated coupling between the different types of motion. Okah-Avae [11] investigated vibrations considering the nonlinearity in stiffness due to open-close mechanisms in cracks. Dimarogonas [12] also studied cracked rotor and health monitoring of rotating structures. R. Siva and others [13] studies the magnetic bearings which supports the rotors without contact and the active dampers.

Analytical approaches are successful for problems with simple geometries to a certain complexity. This pushes researchers to develop and use computational methods to solve the complex structures. Finite element methods were first developed for structural dynamics, and then it was extended to rotor dynamics by many researchers. Ruhl and Booker [14] were of the first to use the FE in rotating structures. Nelson and McVaugh [15] generalized FE techniques to consider various effects such as rotary inertia, gyroscopic moments and axial (thrusting) force. The output of the FE development can solve complex geometries taking into consideration rotary inertia, gyroscopic effect, shear deformation for solid or hollow cross sections, different types of couplings and nonlinear interactions.

The FE simulations of the motion of the spinning shafts produce accurate solution for spatial and temporal dynamics represented by large numerical data. The POD processing the numerical data-bases shall characterize optimally the dynamics into a set of finite coupled modes [16, 17]. The optimal POD modes can be used as bases for model reduction in place of the linear normal modes.

DYNAMICS OF CONTINUOUS ROTOR

Consider a continuous rotor with length l in its deformed configurations as shown in Figure 1. The

global rectangular coordinate system (X_1, X_2, X_3) is a fixed coordinate with X_1 passing through the bearings centerlines. The deflections in X_2 and X_3 directions are denoted by $\upsilon(s,t)$ and $w(s,t)$ respectively. The angles $\theta_2(s,t)$ and $\theta_3(s,t)$ are the projections of the normal to cross section in the deformed configuration (at time $t+\Delta t$) into the X_2, X_1 and X_3, X_1 planes of the reference configuration case (at time t). The kinematic description couples the displacement of the material curve that coincides with the curve passing through the centers of all cross-sections with the displacement of the material planes defined by the cross-section transversal to the middle curve. In the original configuration, the material planes are taken normal to the middle-curve. During deformation, the cross-sections do not remain perpendicular to the displaced middle-curve. Assuming that the cross-sections do not have straining through the thickness, then the motion can be considered to be a coupling between the displacement of the middle curve and the rotation field of the cross-section.

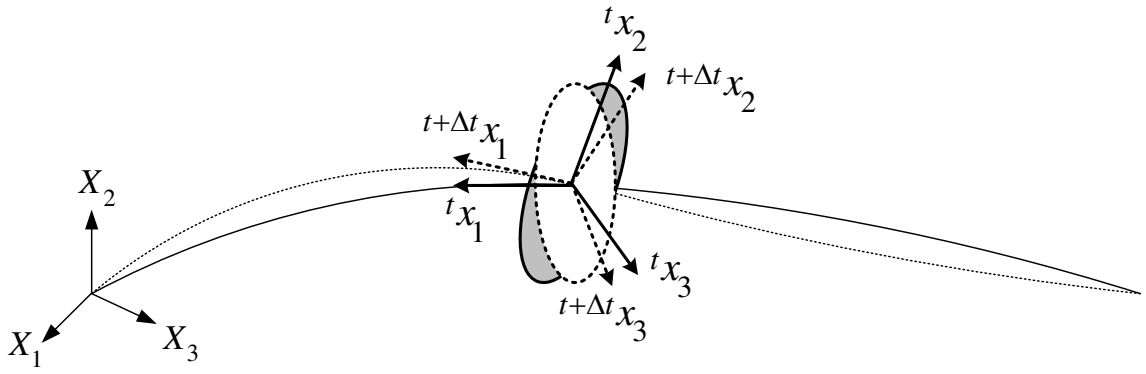

Figure 1. Configurations of the deformed rod at different times.

Let $u_1(s,t), u_2(s,t), u_3(s,t)$ denote the components of the displacement field of the middle curve in the X_1, X_2 and X_3 directions respectively. $r_1(s,t), r_2(s,t), r_3(s,t)$ denote the twisting, and bending components of the rotation field of the cross-section. Then the motion can be described by the vector field:

$$\boldsymbol{U}(s,t) = \left[u_1(s,t), u_2(s,t), u_3(s,t), r_1(s,t), r_2(s,t), r_3(s,t)\right]^T \tag{1}$$

During motion, the displacements and rotations are coupled at different levels to each other. The transverse displacements are coupled to the bending rotations due to shearing and geometric nonlinearity. Sometimes the motion of a rotating shaft is dominated by the bending components of the field. For such cases, there exist linear and nonlinear models that capture the whirling motion of a shaft rotating at constant speed. For example, the following nonlinear equations describe the whirling motions of a shaft with geometric nonlinearity and distributed eccentricity [8]:

$$EI\frac{\partial^4 u_2(s,t)}{\partial s^4}+\rho A\frac{\partial^2 u_2(s,t)}{\partial t^2}-\frac{\rho AR^2}{4}\left(\frac{\partial^4 u_2(s,t)}{\partial s^2\partial t^2}+2\Omega\frac{\partial^3 u_3(s,t)}{\partial s^2\partial t}\right)+c\frac{\partial u_2(s,t)}{\partial t}$$
$$+\frac{EA}{2L}\frac{\partial^2 u_2(s,t)}{\partial s^2}\int_0^L\left[\left(\frac{\partial u_2(s,t)}{\partial s}\right)^2+\left(\frac{\partial u_3(s,t)}{\partial s}\right)^2\right]ds=\rho A\Omega^2\left[e_2(s)Cos(\Omega t)-e_3(s)Sin(\Omega t)\right]$$
$$EI\frac{\partial^4 u_3(s,t)}{\partial s^4}+\rho A\frac{\partial^2 u_3(s,t)}{\partial t^2}-\frac{\rho AR^2}{4}\left(\frac{\partial^4 u_3(s,t)}{\partial s^2\partial t^2}-2\Omega\frac{\partial^3 u_2(s,t)}{\partial s^2\partial t}\right)+c\frac{\partial u_3(s,t)}{\partial t}$$
$$+\frac{EA}{2L}\frac{\partial^2 u_3(s,t)}{\partial s^2}\int_0^L\left[\left(\frac{\partial u_2(s,t)}{\partial s}\right)^2+\left(\frac{\partial u_3(s,t)}{\partial s}\right)^2\right]ds=\rho A\Omega^2\left[e_2(s)Sin(\Omega t)-e_3(s)Cos(\Omega t)\right] \quad (2)$$

where $u_2(s,t), u_3(s,t)$ are the transverse displacements in the X_2 and X_3 directions respectively, EI is the bending rigidity, ρ is the mass density, A is the cross-sectional area and L is the shaft length. The terms e_2 and e_3 are the rotor unbalance in the two transverse directions. c is the damping coefficient and Ω is the shaft spinning speed. In this model, the coupling exists due to the gyroscopic terms and the geometric nonlinearity.

The above model has limited predictability since it cannot predict the dynamic interactions between whirling modes and rigid body modes of motion, and the straining along the shaft. Nonlinear shafts can be studied by reducing the order of the governing equations by restricting them on invariant subspaces in phase space. However, it is possible to derive optimal nonlinear model based on appropriate measure of the energy of motion and its distribution over spatial patterns. This could be obtained from the dynamics of the spinning shaft either computed or measured.

Dynamics of the spinning shaft as seen by POD transform

A nonlinear FE model based on the Updated Lagrange UL formulation with nonlinear strain displacement relationship is appropriate to derive a computation model for small strain and large displacement problems like the spinning shaft. The UL formulation is appropriate for problems undergoing significant geometry changes because of large rotations.

Consider a two-node spatial beam element in FE model. Each node has six-degrees of freedom associated with the axial force, two shear forces, two bending moments and a torque. The discrete numerical results obtained from the solution of the FE model can be arranged in vector field describing the continuous dynamics of the shaft:

$$\boldsymbol{U}(s,t)=\left[u_1(s,t),u_2(s,t),u_3(s,t),r_1(s,t),r_2(s,t),r_3(s,t)\right]^T \quad (3)$$

According to the POD theory [1], the configuration vector field can be expanded optimally into Proper Orthogonal PO modes:

$$\boldsymbol{U}(s,t)=\sum_{m=1}^{M}A_m(t)\sqrt{\lambda_m}\boldsymbol{\Phi}_m(s),\qquad m=1,2,...,M \tag{4}$$

where, $A_m(t)$ representing the response in time (POD mode Amplitude), $\boldsymbol{\Phi}_m(s)$ is the spatial arrangement of the motion (POD mode shape) and λ_m is the participation factor (POD mode energy factor). The norms of the components of a spatial POD mode determine the level of coupling between the various components of the motion. For a rotating shaft, the generic motion involves coupling between displacements and rotations (three displacements and three rotations). The $L2$ norms of the components of a POD mode can be used to determine the strength of coupling between different types of displacements and rotations it can be expressed as:

$$C_{km}=\left\|\Phi_{km}(s)\right\|=\sqrt{\frac{2}{L}\int_0^L\left(\Phi_{km}(s)\right)^2 ds},\qquad k=1,...,6,m=1,...,M \tag{5}$$

The simply supported straight shaft considered in this analysis has length of $1.5m$ and radius $0.01m$. The shaft is made of steel with Young's modulus 193050 MPa, mass density of $7908\ \mathrm{kg}/m^3$ and Poisson's ratio 0.3. The motion of the shaft is excited by a moment that will drive the shaft to spin with a speed higher that the second critical speed in short time (startup) then the moment is released. Releasing the moment (shutdown) decreases the shaft speed gradually and passes through the critical speeds resulting motion with different interactions between the bending and torsion motions. Figure 2 shows plot for the transverse displacement for a point located at the middle of the shaft and another point located at one fourth of the shaft. The simulated dynamics indicates that the shaft was performing pure rotational motion until the transverse motion started to appear when the spinning speed approaches the second critical speed of the shaft producing whirling motion in the second bending mode (Part "A" of Figure-2). In the next phase, the amplitude of transverse motion is reduced and strong interaction between the transverse vibration the torsion (Part "B" of Figure-2) takes place for few seconds. When the shaft speed approaches the first critical speed, whirling motion in the first bending mode with high amplitude (Part "C" of Figure-2) occurs. During all phases, interesting coupling between various deformation modes and coupling among rigid body rotation and twisting-bending modes exist.

In order to understand the dynamic interaction , it is processed by using the Time-POD method for the segment of the trajectory of the motion (6 seconds) in the phases (A, B and C) as shown in Figure 2 .

The POD transform indicates that the dynamics is described by one major mode that contains the biggest value of the energy almost 99.80% of the total auto-correlation energy of the motion.

Moreover, another two modes (the second and third) with equal participation 0.09% of the total energy. And another two modes (fourth and fifth) also have almost equal participation with value of 0.002% of the total auto-correlation energy. The sum of energies of the first five modes is almost 100%, (Table-1).

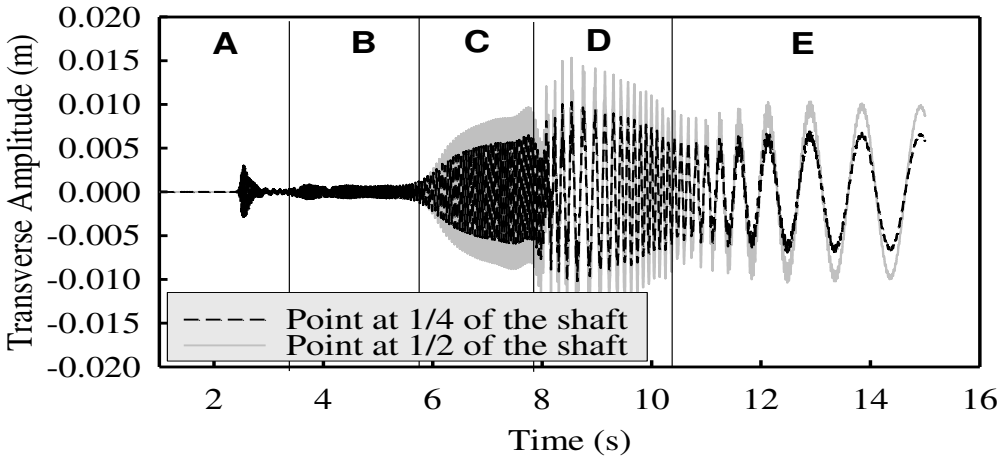

Figure 2. Transverse displacement of the rotating shaft recorded at the middle of the shaft and at one-fourth of the shaft.

Table 1: Auto-correlation energy participation of the first 5 POD modes. And norms of the components of each mode.

m	λ_m	C_{1m}	C_{2m}	C_{3m}	C_{4m}	C_{5m}	C_{6m}
1	0.9980852	0.000058	0.000030	0.000081	0.999990	0.000001	0.000001
2	0.0009411	0.000002	0.925928	0.377684	0.000062	0.000718	0.001713
3	0.0009373	0.000002	0.377694	0.925929	0.000069	0.001713	0.000718
4	0.0000181	0.000040	0.384067	0.923299	0.000225	0.003359	0.001246
5	0.0000180	0.000013	0.923298	0.384067	0.000300	0.001246	0.003359

The amplitudes of the first five POD modes are plotted in Figure-3. The first amplitude (Figure-3 A) represents the shaft angular displacement variation during this time interval. it can be seen that the value of the angular speed reduced in three steps over the whole-time interval. At the first step (almost for 0.75 seconds) the shaft undergoes whirling in the second mode with high amplitude and frequency of 433.5 rad/s (close the frequency of the second normal mode of vibration of the simply supported shaft). Then for the next three seconds a strong interaction between twisting and bending appears together with switching the bending mode from the second to the first. The last three seconds the whirling in the first transverse mode with high amplitude and frequency 108.6 rad/s (almost identical to the natural frequency of the first bending mode for the simply supported shaft) appears. The cross plot between the two amplitudes (“E”) indicates circular motion (Whirling).

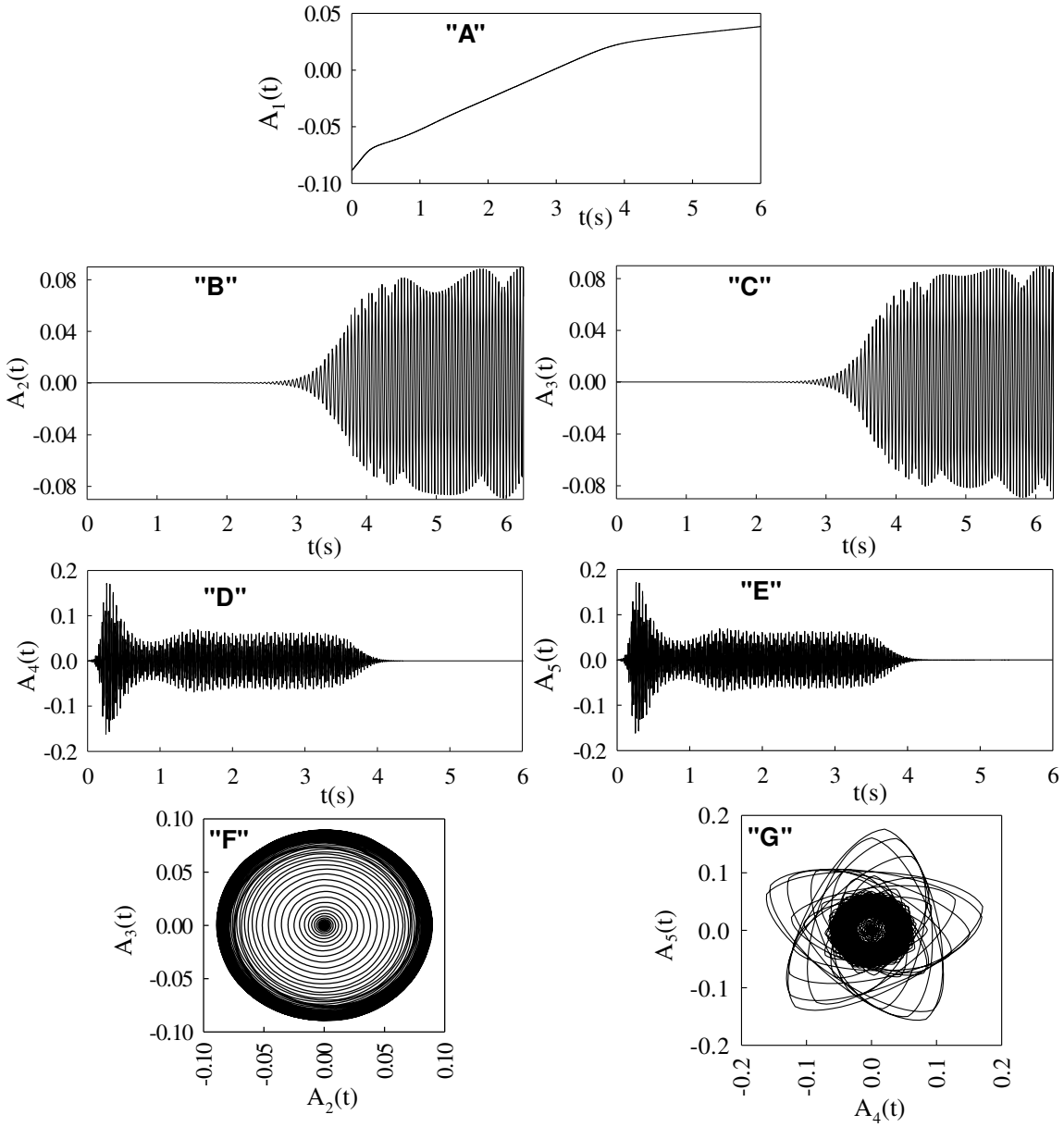

Figure 3: (A to E) Amplitudes of the first five POD modes respectively. "F" is the cross-plot between the second and third amplitudes. "G" is the cross-plot between the fourth and fifth amplitudes.

The normalized shapes of the whirling modes are shown in Figure-4 and the corresponding norms are given in Table-1. The first whirling mode represented by the two POD modes 2 and 3 (Figure-4; A and B) and the second whirling mode represented by the fourth and fifth POD modes (Figure-4; C and D). Both whirling modes are deformation modes coupled to rotations representing the first and second bending modes for the simply supported shaft.

The norm of the POD mode quantifies the interaction between the transverse deformations in X_2 and

X_3 directions. In Table1, the norms magnitude of the second POD mode in X_2 and X_3 directions are 0.925928 and 0.377684 respectively. While norms magnitudes exchanged their values in the third POD mode with the values of 0.377694 in X_2 direction and 0.925929 in X_3 direction. Here it can be concluded that for circular motion two POD modes are required to represent single circular motion (whirling mode).

The fourth and the fifth POD modes (Figure-4; C and D) indicate deformation modes corresponding to the second bending mode of the simply supported shaft. The norms of the fourth POD mode are quantified at 0.384067 and 0.923299 in X_2 and X_3 direction respectively. While the norms of the fifth POD mode are quantified at 0.923298 and 0.384067 in X_2 and X_3 direction respectively. Also, both the fourth and fifth POD modes needed to represent the whirling motion in the second bending mode.

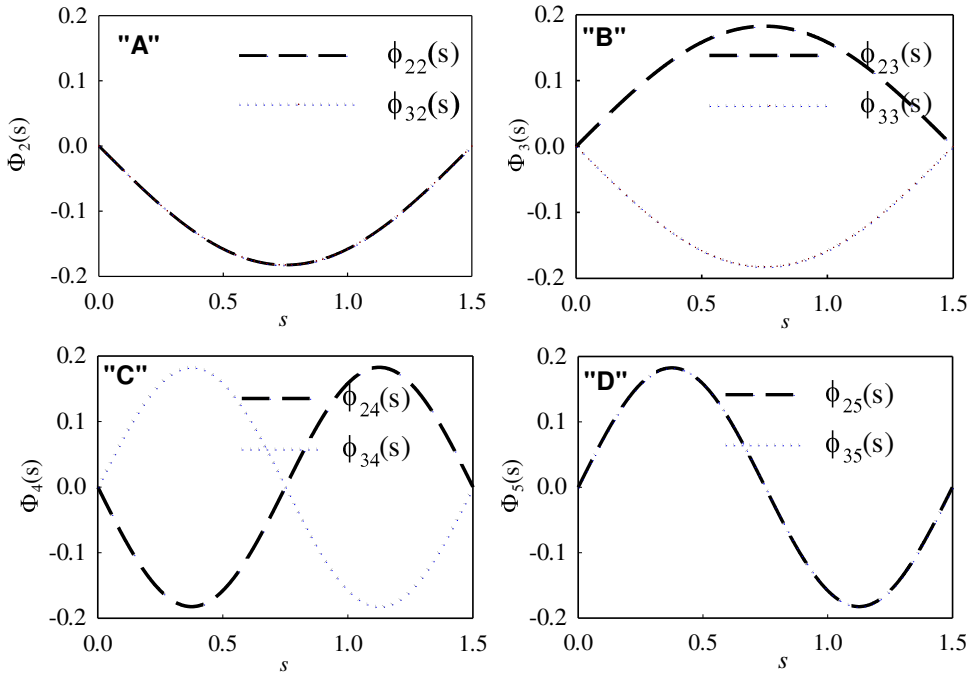

Figure 4: The POD mode shape components of the second and third POD modes (A & B) and the fourth and fifth POD modes (C & D).

In summary, the POD analysis revealed that a motion is composed of a near rigid body mode and a set of pure whirling modes. Each whirling mode required two POD modes to represent its dynamics. The second and third POD modes represents the whirling in the first mode ,the fourth and fifth POD modes together represent the second whirling mode.

Model reduction for rotating shaft

The common method to derive a reduced order model is by projecting the nonlinear model based on linear normal mode shapes. Here will derive the reduced order model using the extracted coupled

POD modes for the rotating shaft studied above. Particularly, we use the eight components of the four POD modes as bases for model reduction.

The nonlinear model described in equations (2) counts for the effects of large shearing, gyroscopic effects due to the rigid body motion of the shaft and nonlinear terms due to large deformations. To derive a reduced order model for the whirling motion we will use the following spatial POD bases as indicated in Figure 4:

$$\boldsymbol{\Phi}_m(s) \equiv \begin{bmatrix} \varphi_{2m}(\mathrm{s}) \\ \varphi_{3m}(s) \end{bmatrix}, m = 2,3,4,5 \tag{6}$$

Projecting the nonlinear partial differential equation of motion for the spinning shaft equation (2) onto the space spanned by the four POD modes yields the following set of four coupled nonlinear oscillators:

$$\left(\alpha_0\mathbf{H}_0 + \alpha_1\mathbf{H}_1\right)\mathbf{Q}_{tt} + \left(\alpha_2\mathbf{H}_2 + \alpha_3\mathbf{H}_3\right)\mathbf{Q}_t + \left(\alpha_4\mathbf{H}_4\right)\mathbf{Q} + \alpha_5\mathbf{H}_1\left\{NL\right\} = \alpha_6\mathbf{F} \tag{7}$$

Where the vectors

$$\begin{aligned} &\mathbf{Q} \equiv \left\{Q_1(t)Q_2(t)Q_3(t)Q_4(t)\right\}^T, \\ &\mathbf{Q}_n \equiv \left\{Q_n(t)Q_n(t)Q_n(t)Q_n(t)\right\}^T, n = 1,2,3,4 \end{aligned} \tag{8}$$

And the

$$NL = \begin{cases} C_1\mathbf{Q}_1 \circ \mathbf{Q} \circ \mathbf{Q}_1 + C_2\mathbf{Q}_2 \circ \mathbf{Q} \circ \mathbf{Q}_2 + 4C_3\mathbf{Q}_3 \circ \mathbf{Q} \circ \mathbf{Q}_3 + 4C_4\mathbf{Q}_4 \circ \mathbf{Q} \circ \mathbf{Q}_4 \\ +2C_5\mathbf{Q} \circ \mathbf{Q}_1 \circ \mathbf{Q}_2 + 4C_6\mathbf{Q} \circ \mathbf{Q}_1 \circ \mathbf{Q}_3 + 4C_7\mathbf{Q} \circ \mathbf{Q}_1 \circ \mathbf{Q}_4 \\ +4C_8\mathbf{Q} \circ \mathbf{Q}_2 \circ \mathbf{Q}_3 + 4C_9\mathbf{Q} \circ \mathbf{Q}_2 \circ \mathbf{Q}_4 + 8C_{10}\mathbf{Q} \circ \mathbf{Q}_3 \circ \mathbf{Q}_4 \end{cases} \tag{9}$$

Where the $\circ$ is the Hadamard product [18], and the force vector

$$\mathbf{F} = \begin{bmatrix} -c_{22} & c_{32} \\ -c_{23} & c_{33} \end{bmatrix}\begin{bmatrix} e_2 \\ e_3 \end{bmatrix}\cos(\Omega t) + \begin{bmatrix} -c_{32} & c_{22} \\ -c_{33} & c_{23} \end{bmatrix}\begin{bmatrix} e_2 \\ e_3 \end{bmatrix}\sin(\Omega t) \tag{10}$$

And constants related to the POD:

$$\begin{aligned} &C_1 = \left(c_{22}^2 + c_{32}^2\right), C_2 = \left(c_{23}^2 + c_{33}^2\right), C_3 = \left(c_{24}^2 + c_{34}^2\right), C_4 = \left(c_{25}^2 + c_{35}^2\right), \\ &C_5 = \left(c_{22}c_{23} + c_{32}c_{33}\right), C_6 = \left(c_{22}c_{24} + c_{32}c_{34}\right), C_7 = \left(c_{22}c_{25} + c_{32}c_{35}\right) \\ &C_8 = \left(c_{23}c_{24} + c_{33}c_{34}\right), C_9 = \left(c_{23}c_{25} + c_{33}c_{35}\right), C_{10} = \left(c_{24}c_{25} + c_{34}c_{35}\right) \end{aligned} \tag{11}$$

While the matrices

$$\mathbf{H}_0 = \mathbf{H}_2 = \begin{pmatrix} C_1 & C_5 & 0 & 0 \\ C_5 & C_2 & 0 & 0 \\ 0 & 0 & C_3 & C_{10} \\ 0 & 0 & C_{10} & C_4 \end{pmatrix}, \mathbf{H}_1 = \begin{pmatrix} C_1 & C_5 & 0 & 0 \\ C_5 & C_2 & 0 & 0 \\ 0 & 0 & 4C_3 & 4C_{10} \\ 0 & 0 & 4C_{10} & 4C_4 \end{pmatrix}$$

$$\mathbf{H}_3 = \begin{pmatrix} 0 & -\left(c_{23}c_{32} - c_{22}c_{33}\right) & 0 & 0 \\ \left(c_{23}c_{32} - c_{22}c_{33}\right) & 0 & 0 & 0 \\ 0 & 0 & 0 & -4\left(c_{25}c_{34} - c_{24}c_{35}\right) \\ 0 & 0 & 4\left(c_{25}c_{34} - c_{24}c_{35}\right) & 0 \end{pmatrix} \tag{12}$$

$$\mathbf{H}_4 = \begin{pmatrix} C_1 & C_5 & 0 & 0 \\ C_5 & C_2 & 0 & 0 \\ 0 & 0 & 16C_3 & 16C_{10} \\ 0 & 0 & 16C_{10} & 16C_4 \end{pmatrix}$$

and the constant coefficients $\alpha_K, K = 0,..,6$ are related to the shaft material and geometric properties as follows:

$$\begin{aligned} &\alpha_0 = \frac{1}{2} L\pi R^2 \rho, \alpha_1 = \frac{\pi^3 R^4 \rho}{8L}, \alpha_2 = \frac{cL}{2}, \alpha_3 = \frac{\pi^3 R^4 \rho\Omega}{4L}, \\ &\alpha_4 = \frac{E\pi^5 R^4}{8L^3}, \alpha_5 = -\frac{E\pi^5 R^2}{8L^3}, \alpha_6 = 2LR^2 \rho\Omega^2 \end{aligned} \tag{13}$$

and the corresponding norms are:

Table 2: Norms of the POMs used to in the reduced model.

m	c_{2m}	c_{3m}
2	- 925928	-0.377684
3	0.377694	-0.925929
4	0.384060	-0.923299
5	0.923298	0.384067

and the matrices $\mathbf{H}_K, K = 0,...,4$ are the matrices that contains the POD norms

$$\mathbf{H}_3 = \begin{pmatrix} 0. & -1.0 & 0. & 0. \\ 1.0 & 0. & 0. & 0. \\ 0. & 0. & 0. & 4.0 \\ 0. & 0. & -4.0 & 0. \end{pmatrix}, \mathbf{H}_4 = \begin{pmatrix} 1.0 & 0. & 0. & 0. \\ 0. & 1.0 & 0. & 0. \\ 0. & 0. & 16.0 & 0. \\ 0. & 0. & 0. & 16.0 \end{pmatrix} \tag{14}$$

$$\begin{aligned} &\alpha_0 = 1.8634, \alpha_1 = 0.0002, \alpha_2 = 0.75c, \alpha_3 = 0.0004\Omega \\ &\alpha_4 = 21880.4074, \alpha_5 = -2.1880 \times 10^8, \alpha_6 = 2.37252\Omega^2 \end{aligned} \tag{15}$$

Again, we notice that there are some factors that depend on the shaft spinning speed. Next will study this reduced model by considering both the linearized and nonlinear cases.

Numerical Integration for Reduced Order Model

To study the linearized and nonlinear reduced system numerically, cast it in coupled system of first order ordinary differential equations:

$$\dot{\mathbf{Y}} = \mathbf{AY}, \tag{16}$$

where,

$$\begin{aligned} &\mathbf{Y} \equiv \left[Y_1, Y_2, Y_3, Y_4, Y_5, Y_6, Y_7, Y_8\right]^T \\ &Y_1 = Q_1(t), Y_2 = Q_{1t}(t), Y_3 = Q_2(t), Y_4 = Q_{2t}(t) \\ &Y_5 = Q_3(t), Y_6 = Q_{3t}(t), Y_7 = Q_4(t), Y_8 = Q_{4t}(t) \end{aligned} \tag{17}$$

This system of ordinary differential equations can be solved numerically by the Gear BDF method. The transverse displacement of the center of the shaft at middle span is given by the relations:

$$\begin{Bmatrix} U_2 \\ U_3 \end{Bmatrix} = \begin{bmatrix} c_{22} & c_{32} \\ c_{23} & c_{33} \end{bmatrix} \begin{Bmatrix} Q_1(t) \\ Q_2(t) \end{Bmatrix} + \begin{bmatrix} c_{24} & c_{34} \\ c_{25} & c_{35} \end{bmatrix} \begin{Bmatrix} Q_3(t) \\ Q_4(t) \end{Bmatrix} \tag{18}$$

Testing Reduced Order Model

The derived reduced order will be tested applying several operational conditions. Comparison between the linearized and nonlinear models will be performed.

Initially, the shaft dynamics will be excited by small initial displacement in the U_2 direction $Q_2(t=0) = 0.0001$ and preventing the shaft from rotation ($\Omega = 0$). The shaft shall behave as simply supported rod vibrating freely (necessarily in the first natural frequency). Since the initial displacement applied at the middle point of the shaft is small, no nonlinear behavior will appear. Figure 5 shows the test results for the linear and nonlinear models. Apparently, the shaft has the same response since the geometric nonlinearities are not excited. The vibrations frequency is equal to the first natural frequency of the simply supported rod at 17.8 Hz.

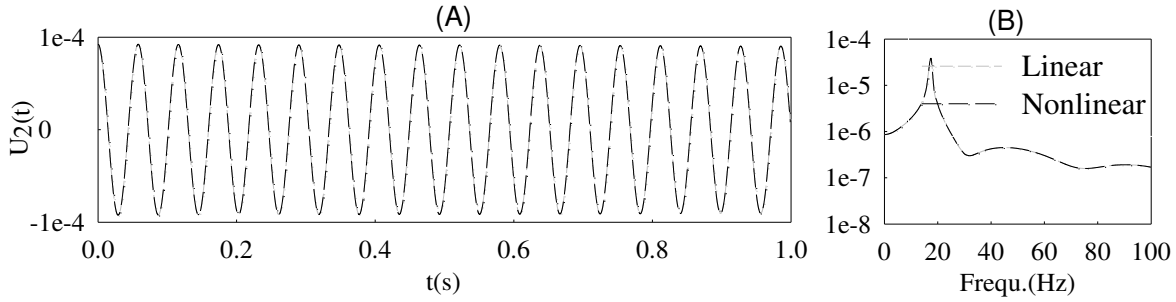

Figure 5. The transverse displacement of a point at the middle of the shaft (A) due to small initial displacement and (B) the FFT results**.**

Then the shaft is driven by a speed close to the first critical speed with presence of eccentricity. Figure 6 shows the whirling in the first mode.

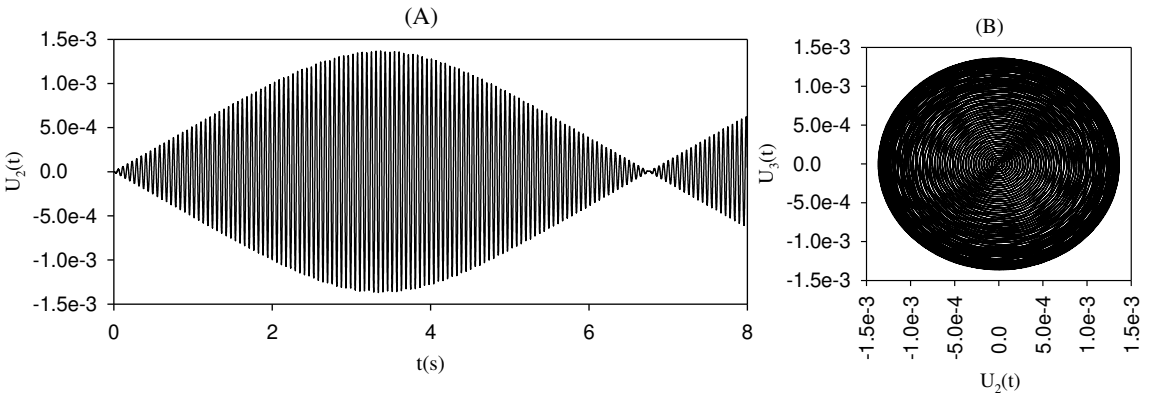

Figure 6. Response due to operational speed closed to the first critical speed. (A) The transverse displacement, (B) the cross plot.

Next, the shaft dynamics excited by spinning it with speed close to the second natural frequency of the shaft in bending, $\Omega = 400 rad/\sec$ (results are shown in Figure 7). The whirling motion in the second bending mode is captured. Comparison between the linear and the nonlinear models are plotted.

Finally, the shaft put into motion by increasing the angular velocity starting from zero and increasing linearly with time. The results are shown in Figure 8 where the shaft spins without deflection until it approaches the first critical speed where the whirling will take place. The cross plot between the two transverse motions indicates the whirling.

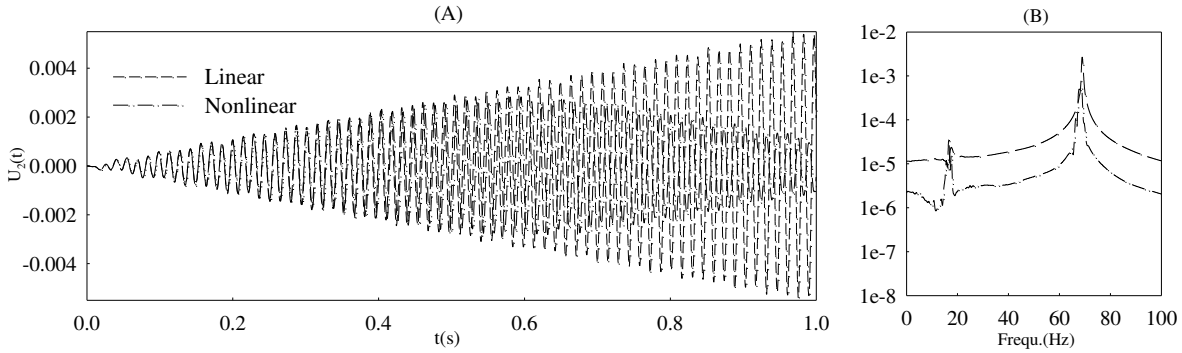

Figure 7. The response of the shat for operational speed close to second critical speed: (A) The transverse displacement, (B) the FFT.

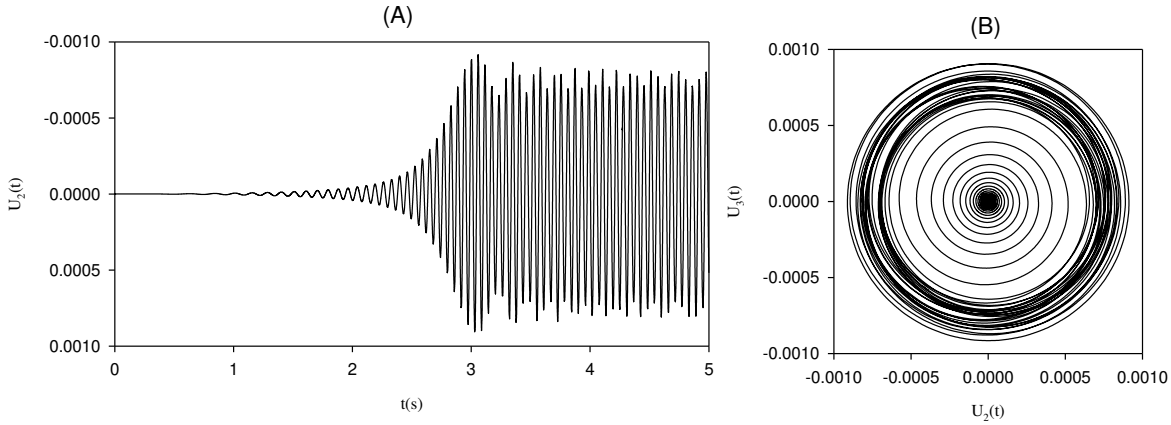

Figure 8. the response of the shaft due to variable spinning speed started from zero and increased to reach the resonance (whirling).

The Time Proper Orthogonal Decomposition transform was used to process the numerical solution of a spinning shaft. The numerical solution was generated using the nonlinear finite elements methods. Processing the dynamics or the rotating shaft using the POD transform identifies the coupling between the rigid body motion due to large rotations, and the elastic bending due to whirling. The whirling motion characterized by pairs of POD modes with equal energy.

Two pairs of the POD modes are used as bases to derive nonlinear reduce order model. The POD norms appear in the reduced model providing weighing values for the interaction between the two transverse motions of the shaft. The reduced order model tested under various conditions and compared to the linear one. The results indicate the effectiveness of the reduced order model to capture the whirling of the shaft.

AKNOLEDGMENT

This work was supported by the National Technical University of Athens (NTUA), and the Applied Science Private University (ASPU).

Compliance with ethical standard

This chapter does not contain any studies with human participants or animals performed by any of the authors.

Conflict of interest

The authors declare that they have no con-flict of interest.

REFERENCES

1. Georgiou, I. Advanced Proper Orthogonal Decomposition Tools: Using Reduced Order Models to Identify Normal Modes of Vibration and Slow Invariant Manifolds in the Dynamics of Planar Nonlinear Rods. *Nonlinear Dyn* **41,** 69–110 (2005). https://doi.org/10.1007/s11071-005-2793-
2. Georgiou, I. T., 2004. Identification of Normal Modes of Vibration of Coupled Infinite-imensional Systems, Proceedings to Euromech 475 Colloquium on Normal Modes of Vibrating System, June 6-9, 2004, Frejus, France.
3. M.D. Al-Ansary, Flexural vibrations of rotating beams considering rotary inertia, Computers & Structures, Volume 69, Issue 3, 1998, Pages 321-328, ISSN 0045-7949, https://doi.org/10.1016/S0045-7949(98)00134-5
4. Bazehhour, B.G., Mousavi, S.M. & Farshidianfar, A. Free vibration of high-speed rotating Timoshenko shaft with various boundary conditions: effect of centrifugally induced axial force. *Arch Appl Mech* **84,** 1691–1700 (2014). https://doi.org/10.1007/s00419-013-0762-5
5. Franklin Y. Cheng, Chris P. Pantelides, Static Timoshenko Beam-Columns on Elastic Media, Journal of Structural Engineering Vol. 114, Issue 5 (May 1988), https://doi.org/10.1061/(ASCE)0733-9445(1988)114:5(1152)
6. H. El-Absy, A.A. Shabana, COUPLING BETWEEN RIGID BODY AND DEFORMATION MODES, Journal of Sound and Vibration, Volume 198, Issue 5,1996, Pages 617-637, ISSN 0022-460X, https://doi.org/10.1006/jsvi.1996.0592.
7. H. H. Yoo, R. R. Ryan and R. A. Scot 1995. Dynamics of flexible beams undergoing large overall motions. Journal of Sound and vibration 181, 261-278.
8. Yamamoto, T., Ishida, Y., 2012: Linear and Nonlinear Rotordynamics: A Modern Treatment with Applications. Wiley, New York. ISBN: 978-3-527-40942-6.
9. Tondl, A., Some Problems of Rotor Dynamics (1965), Czechoslovak Academy of Sciences.
10. Ehrich, F.F. Nonlinear phenomena in dynamic response of rotors in anisotropic mounting systems, Special 50th Anniversary Design Issue, 117, 154-161, (1995)
11. Okah-Avae, B.E., and Mbonu, 0.1. Computer analog digital simulation of a complex mechanical system, Simulation, 37 (2), 47-53, (1981).
12. Dimarogonas, A. D. Vibration of cracked structures: A state of the art review. Engineering Fracture Mechanics. 55, 5, 831-857.
13. R. Siva Srinivasa, R. Tiwaria, Ch. Kannababub. Application of active magnetic bearings in

flexible rotordynamic systems – A state-of-the-art review, Mechanical Systems and Signal Processing, Volume 106, June 2018, Pages 537-572

14. Ruhl, R. L., and Booker, J. F. (February 1, 1972). "A Finite Element Model for Distributed Parameter Turborotor Systems." ASME. *J. Eng. Ind*. February 1972; 94(1): 126–132. https://doi.org/10.1115/1.3428101 94(1):126
15. Nelson, H. D., and McVaugh, J. M. (May 1, 1976). "The Dynamics of Rotor-Bearing Systems Using Finite Elements." ASME. J. Eng. Ind. May 1976; 98(2): 593–600. https://doi.org/10.1115/1.3438942
16. Georgiou, I. T, & Bani-Khaled, MA. "Identifying the Shapes of Coupled Vibrations and Deriving Reduced Order Models for Nonlinear Shafts: A Finite Element-Proper Orthogonal Decomposition Approach." Proceedings of the ASME 2004 International Mechanical Engineering Congress and Exposition. Dynamic Systems and Control, California, USA. November 13–19, 2004. pp. 877-885. ASME. https://doi.org/10.1115/IMECE2004-60015.
17. Georgiou, I. T, & Bani-Khaled, MA. "Extracting Signatures for Rigid Body Motion and Modes of Coupled Vibration in Elastic Multi-Rod Mechanisms by POD Processing of the Finite Element Dynamics." Proceedings of the ASME 2003 International Design Engineering Technical Conferences and Computers and Information in Engineering Conference. Volume 5: 19th Biennial Conference on Mechanical Vibration and Noise, Parts A, B, and C. Chicago, Illinois, USA. September 2–6, 2003. pp. 53-62. ASME. https://doi.org/10.1115/DETC2003/VIB-48309
18. K.J. Horadam, Hadamard Matrices and Their Applications, Princeton University Press, Princeton, New Jersey (2006).

Figures

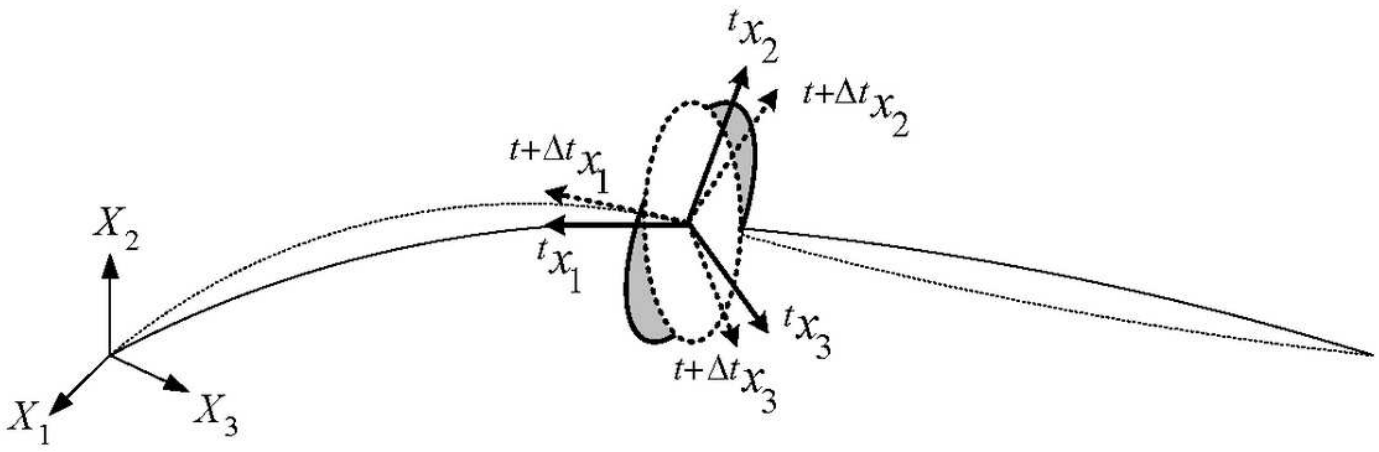

Figure 1

Configurations of the deformed rod at different times.

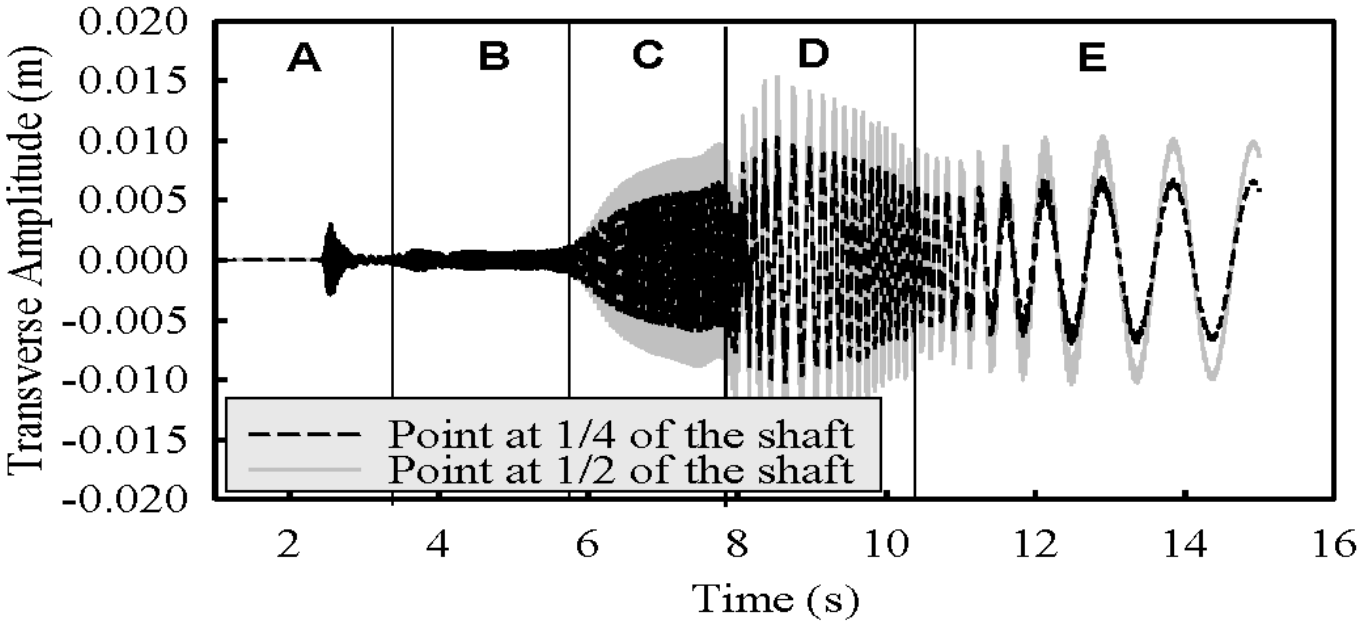

Figure 2

Transverse displacement of the rotating shaft recorded at the middle of the shaft and at one-fourth of the shaft.

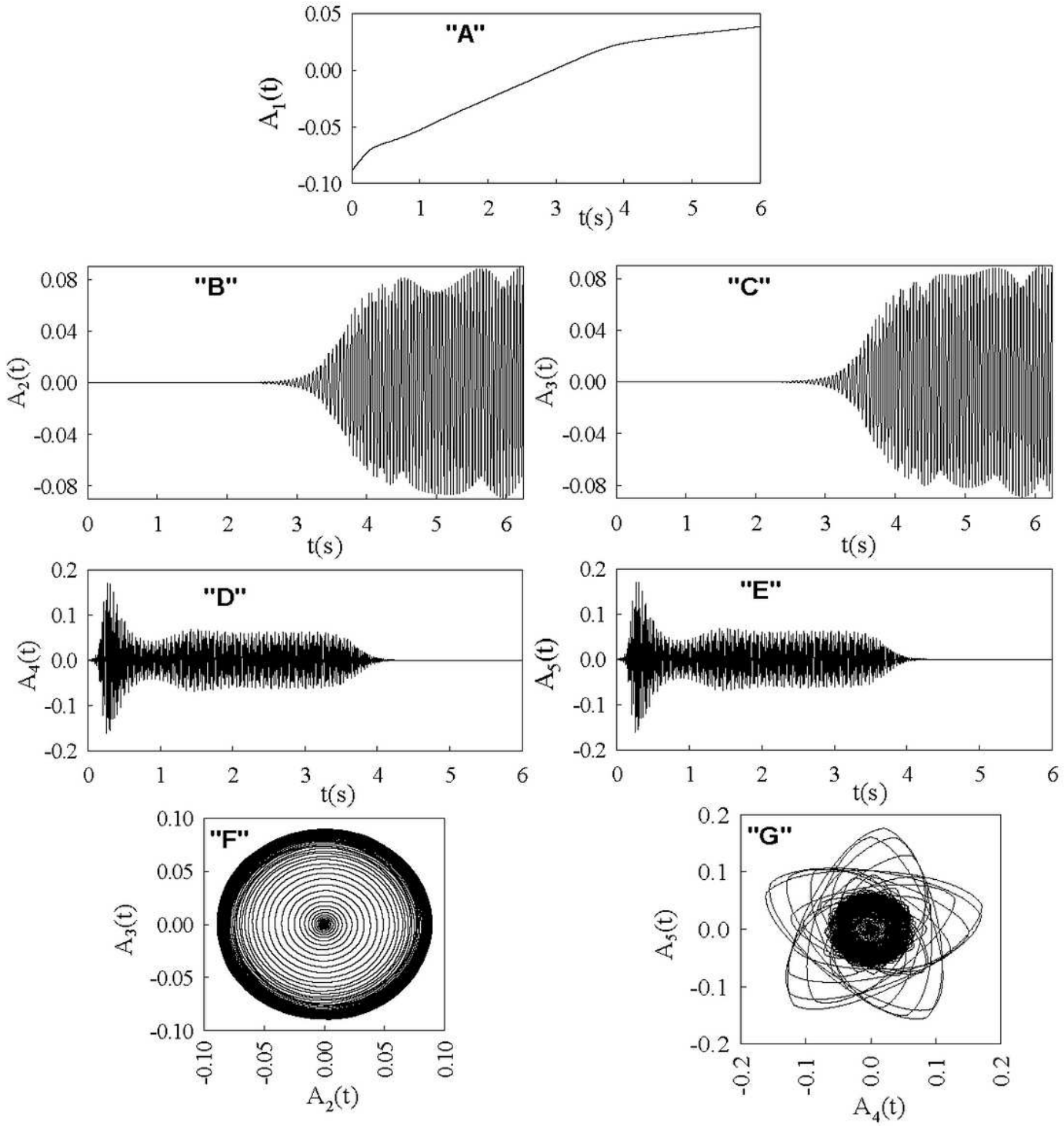

Figure 3

(A to E) Amplitudes of the first five POD modes respectively. “F” is the cross-plot between the second and third amplitudes. “G” is the cross -plot between the fourth and fifth amplitudes.

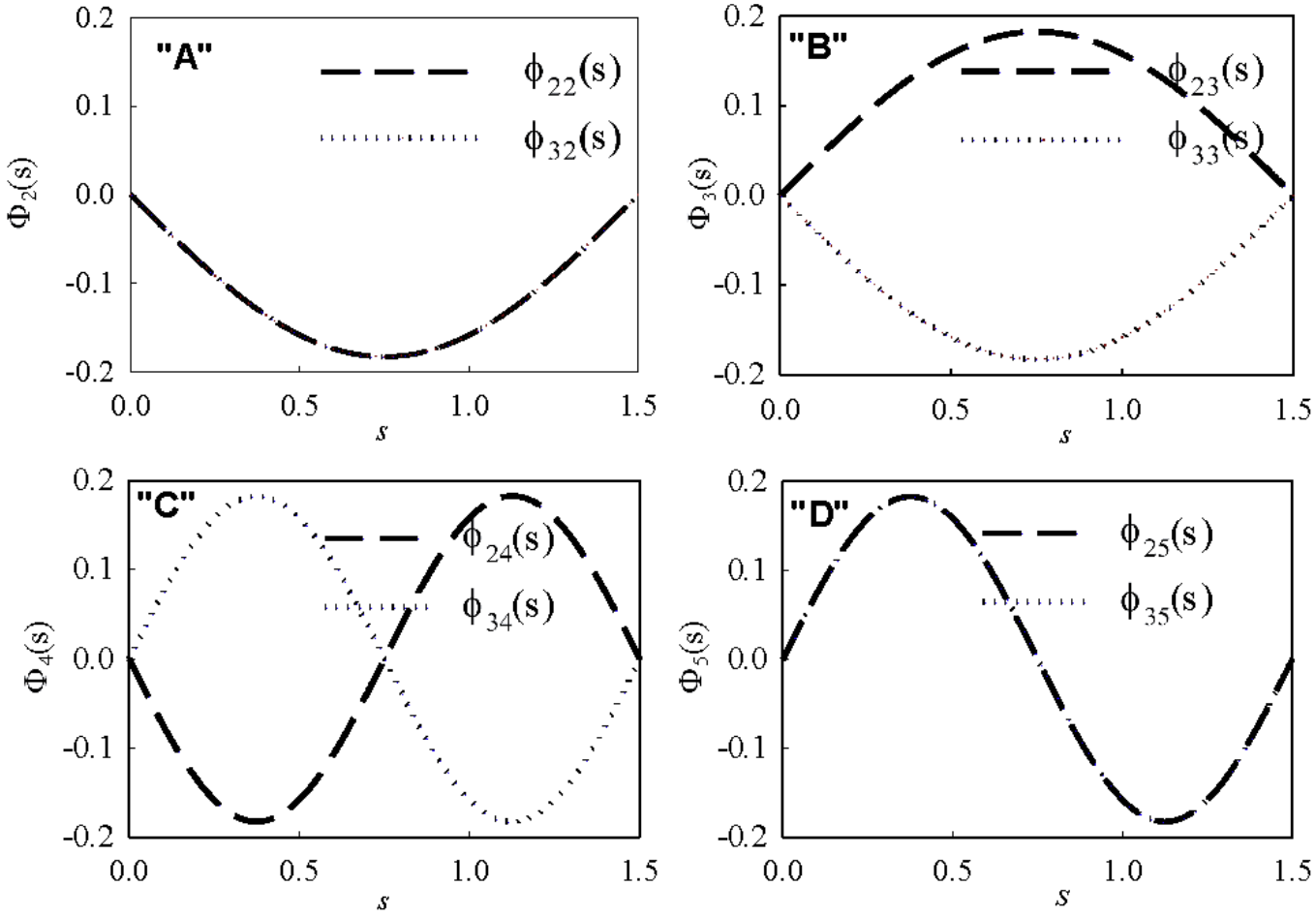

Figure 4

The POD mode shape components of the second and third POD modes (A & B) and the fourth and fifth POD modes (C & D).

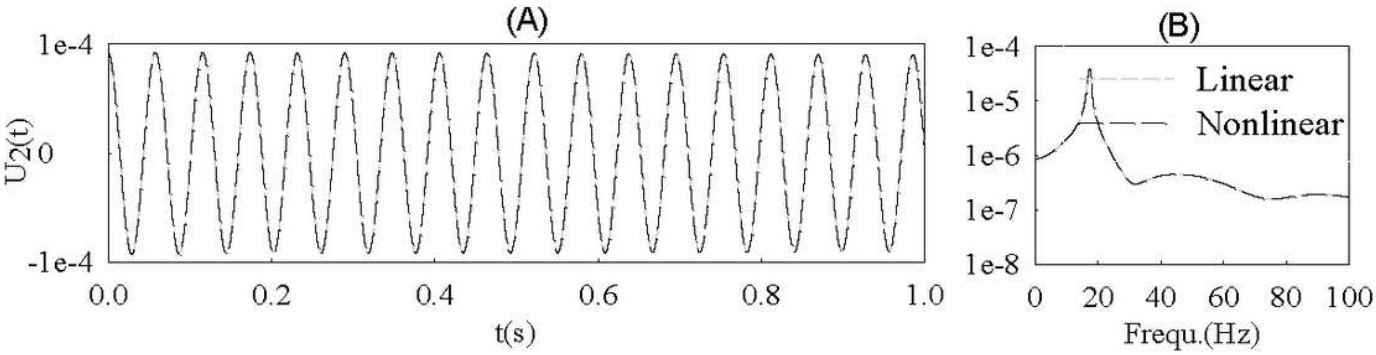

Figure 5

The transverse displacement of a point at the middle of the shaft (A) due to small initial displacement and (B) the FFT results.

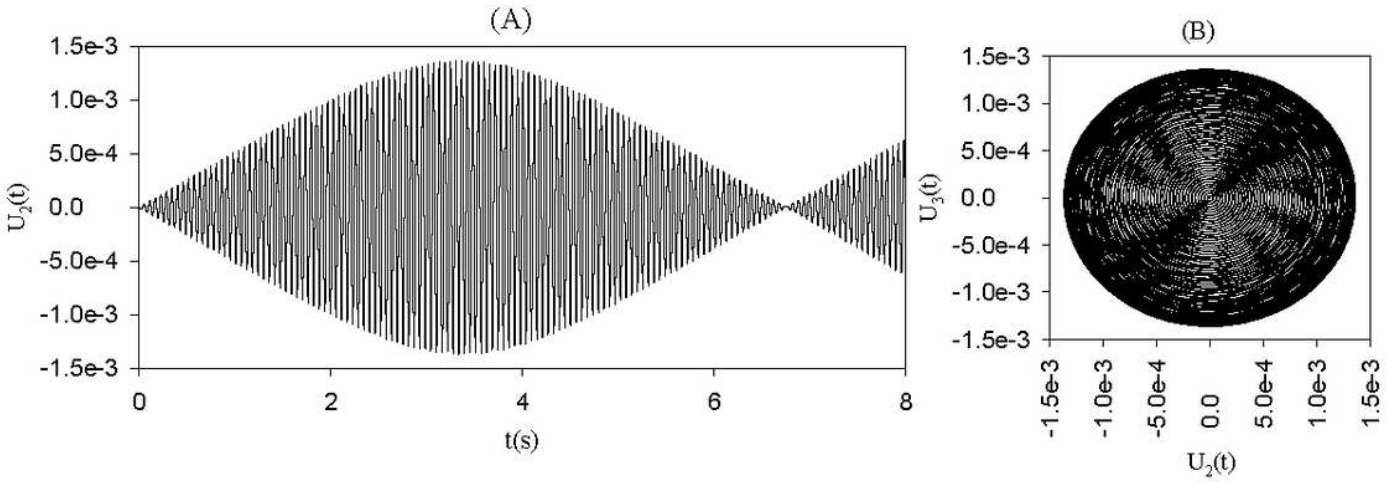

Figure 6

Response due to operational speed closed to the first critical speed. (A) The transverse displacement, (B) the cross plot.

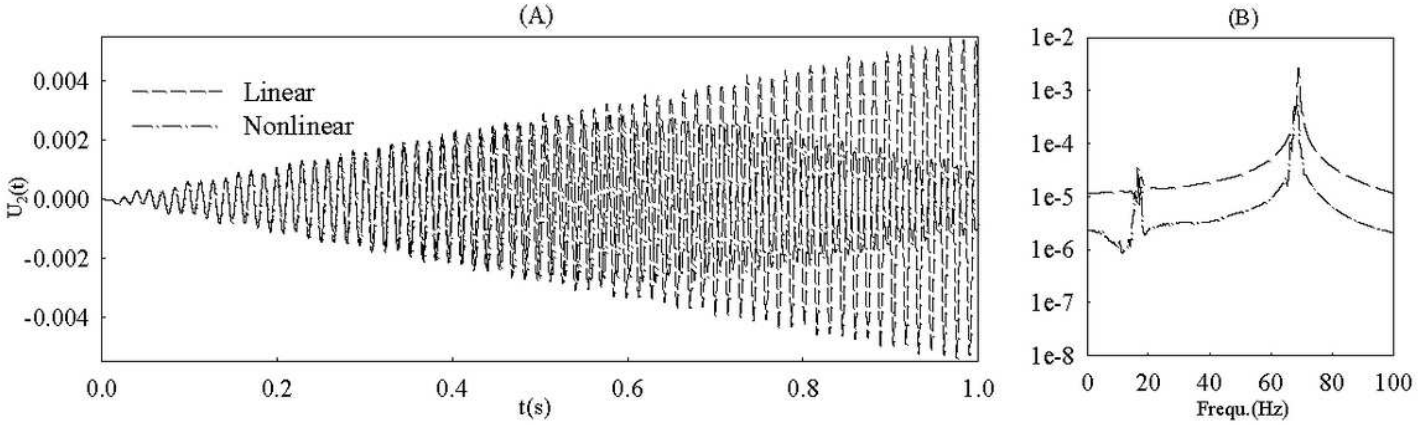

Figure 7

The response of the shat for operational speed close to second critical speed: (A) The transverse displacement, (B) the FFT.

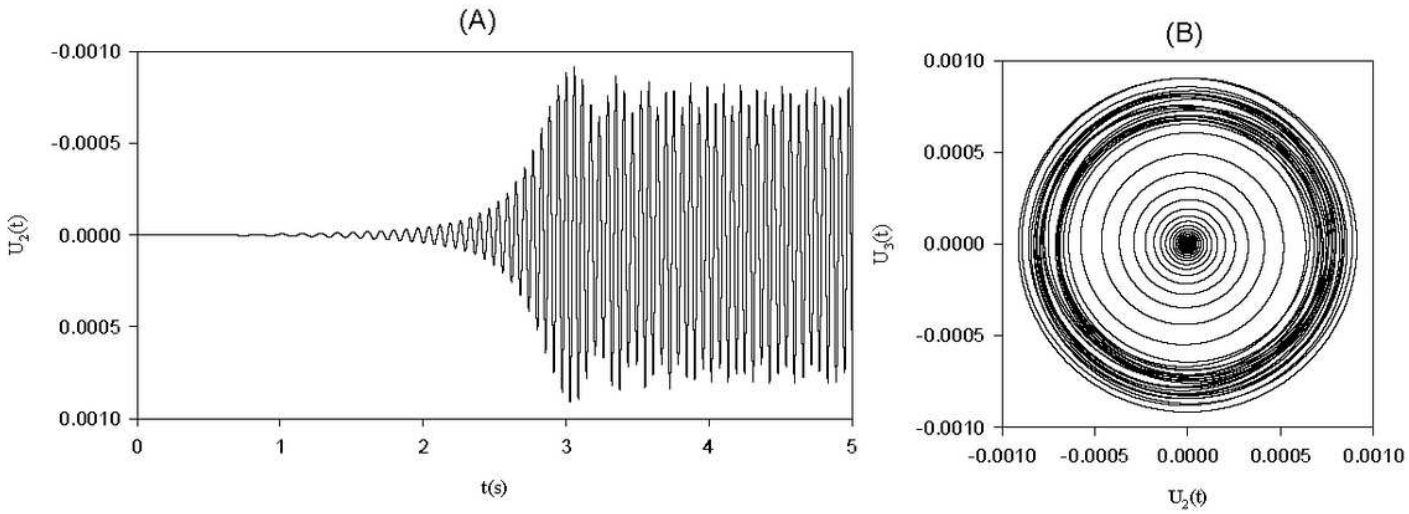

Figure 8

the response of the shaft due to variable spinning speed started from zero and increased to reach the resonance (whirling).